Bubble geobarometry: A record of pressure changes, degassing, and regassing at Mono Craters, California

James M. Watkins[1]*, Michael Manga[1], and Donald J. DePaolo[1,2]
[1]Department of Earth and Planetary Science, University of California–Berkeley, Berkeley, California 94720-4767, USA
[2]Lawrence Berkeley National Laboratory, Berkeley, California 94720, USA

ABSTRACT

Water concentration profiles around bubbles offer a new kind of geobarometer. We measure H_2O and CO_2 concentrations in glass adjacent to bubbles in pyroclastic obsidian from Mono Craters, California (United States). H_2O and CO_2 concentration gradients are preserved during the eruption and record nonequilibrium degassing. A key result is that H_2O is enriched in the glass surrounding the bubbles, indicating that bubbles were resorbing into the melt just prior to the eruption. The required pressure increase for the observed water enrichment is inferred to be the last in a series of pressure cycles with amplitude 5–30 MPa that are caused by repeated fragmentation and annealing. CO_2 concentrations vary substantially in individual obsidian clasts, suggesting that slow diffusion of CO_2 and nonequilibrium degassing contributes to high CO_2/H_2O ratios in pyroclastic obsidian from Mono Craters. These data are direct evidence for vapor-melt disequilibrium and demonstrate that degassing paths from a single parental melt need not be unidirectional. Hence volatile concentration gradients offer a tool for evaluating degassing models and inferring time scales of magmatic processes.

INTRODUCTION

The discharge rate during volcanic eruptions depends on the amount and rate of volatile exsolution, and the efficiency of gas removal from rising magma. Although methods exist to estimate the total volatile budget of volcanic systems, it is more difficult to get information about the relative rates of exsolution versus gas loss during ascent. Volcanic tephra deposits typically contain fragments of quenched glass that preserve pre-eruptive and syneruptive volatile concentrations and thus provide some of the only clues about the physical processes that govern gas loss in the conduit system (e.g., Newman et al., 1988; Roggensack et al., 1997; Spilliaert et al., 2006; Johnson et al., 2008; Bachmann et al., 2009; Blundy et al., 2010).

The concentration of dissolved volatile species (mainly H_2O and CO_2) in silicate melt depends mainly on pressure, with a lesser dependence on temperature, magma composition, and vapor phase chemistry (Liu et al., 2005). In general, as magma rises, pressure decreases until the volatile phase becomes supersaturated and bubbles form. Bubble nucleation and growth, however, may be limited by diffusion in the magma, leading to volatile supersaturation in the host melt or glass (Navon et al., 1998; Gonnermann and Manga, 2005).

The content of dissolved volatiles is conventionally measured on individual spots of vesicle-free glass, and data are compared among many samples from a deposit (Fig. 1). These data sets are often used to constrain volatile contents of the magmas and surrounding gases, assuming that the magma and its bubbles are always in equilibrium (green, blue, and black curves in Fig. 1). However, if diffusion prevents the bubbles from growing or shrinking fast enough to maintain equilibrium (red curve in Fig. 1), volatile concentration gradients may be preserved in the glass and may provide additional information about the timing and rate of gas loss. Here we focus on detecting and characterizing gradients in dissolved volatile concentrations in vesicle-bearing obsidian clasts. The idea is that, because pressure changes (ΔP) lead to bubble growth or resorption, the sign and magnitude of pressure changes can be inferred from H_2O or CO_2 concentration profiles adjacent to bubbles. In samples where volatile concentration profiles are preserved through quench, this geobarometer can be used to calculate time scales of ΔP events in the volcanic conduit.

GEOLOGIC SETTING AND SAMPLE SELECTION

Mono Craters, California (United States), is a 17 km chain of rhyolitic tephra deposits and domes on the eastern flank of the central Sierra Nevada. The most recent, ca. A.D. 1340, eruption at Mono Craters consisted of 0.2 km^3 of pyroclastic fall, flow, and surge deposits, which occurred over a time frame of months, followed by extrusion of 0.4 km^3 distributed among five lava domes and coulees (Sieh and Bursik, 1986). The tephra deposits contain centimeter-scale clasts of white lineated pumice, gray microvesicular obsidian, and black vesicle-free obsidian (Sieh and Bursik, 1986). Our focus is on the vesicle-free obsidian fragments, which are interpreted to sample the margins of magmatic conduits and feeder dikes that were fragmented and incorporated into the eruptive products (Newman et al., 1988).

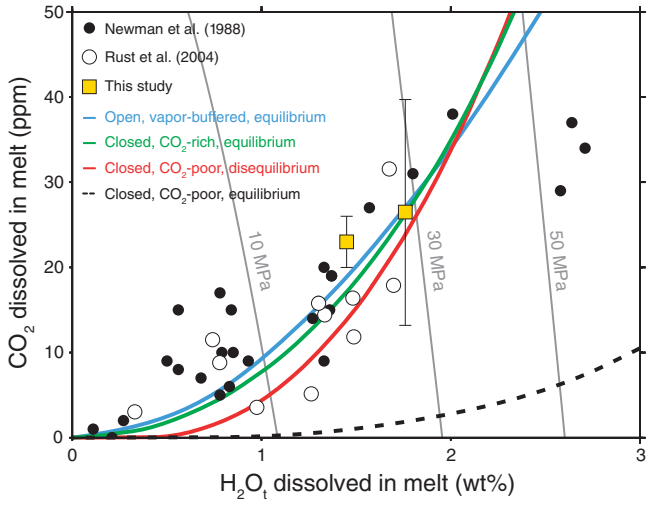

Figure 1. CO_2 versus H_2O for Mono Craters (California, United States) pyroclasts. Circles represent spot analyses on obsidian clasts. Squares represent transects and error bars show the wide variation in CO_2 within individual clasts (see the Data Repository [see footnote 1]). Gray lines represent equilibrium solubilities at 850 °C (Newman and Lowenstern, 2002). Models of degassing commonly assume progressive volatile depletion of single parental melt through bubble growth and gas escape. Volatile concentration data are compared to degassing paths for (1) open-system degassing, where vapor is continuously removed from melt, and (2) closed-system degassing, where volatiles accumulate in bubbles and remain in chemical contact with melt. For either end member, it is possible for degassing to proceed under equilibrium or nonequilibrium conditions. The range of possible degassing paths from open to closed system and equilibrium to nonequilibrium is difficult to resolve from existing data sets on sample suites. Blue curve is from Rust et al. (2004). Red, green, and black curves were digitized from figure 6f of Gonnermann and Manga (2005). Initial H_2O and CO_2 contents, respectively, are as follows: blue: 4 wt% and 282 ppm; green: 4.6 wt% and 14,000 ppm; red: 4.6 wt% and 387 ppm; black: 4.6 wt% and 387 ppm.

*E-mail: jwatkins@berkeley.edu.

Tephra samples were collected from a pit dug at site bb (described in Newman et al., 1988), and several obsidian clasts were selected for analysis. As we are interested in volatile concentrations around bubbles, ideal samples contain bubbles that are relatively large (>0.5 mm), undeformed, and isolated from other bubbles. These samples are rare, yet a couple of candidates were found out of many hundreds of clasts inspected. Wafers of obsidian were prepared for synchrotron-source Fourier transform infrared spectroscopy analysis (see the GSA Data Repository[1]).

H_2O AND CO_2 GRADIENTS AROUND BUBBLES

Figure 2 shows H_2O and CO_2 concentration profiles along three transects perpendicular to two slightly deformed bubbles, bubble A and bubble B, respectively. The chemical gradients provide clear evidence that the bubbles and the surrounding liquid were not in equilibrium with respect to H_2O and CO_2 concentrations at the time the melt quenched. The essential observation is that H_2O content generally increases toward the bubble rims. Bubble B is surrounded by a shell of smaller bubbles, suggesting that H_2O concentration was once greatest where the smaller bubbles nucleated.

The CO_2 profiles are more complicated. Around bubble A, CO_2 is heterogeneous in the matrix, but generally decreases toward the bubble rim in a manner that is not predicted by any model for growth or dissolution of a single bubble (Prousevitch et al., 1993; Prousevitch and Sahagian, 1998; Gonnermann and Manga, 2005). Around bubble B, CO_2 is relatively uniform.

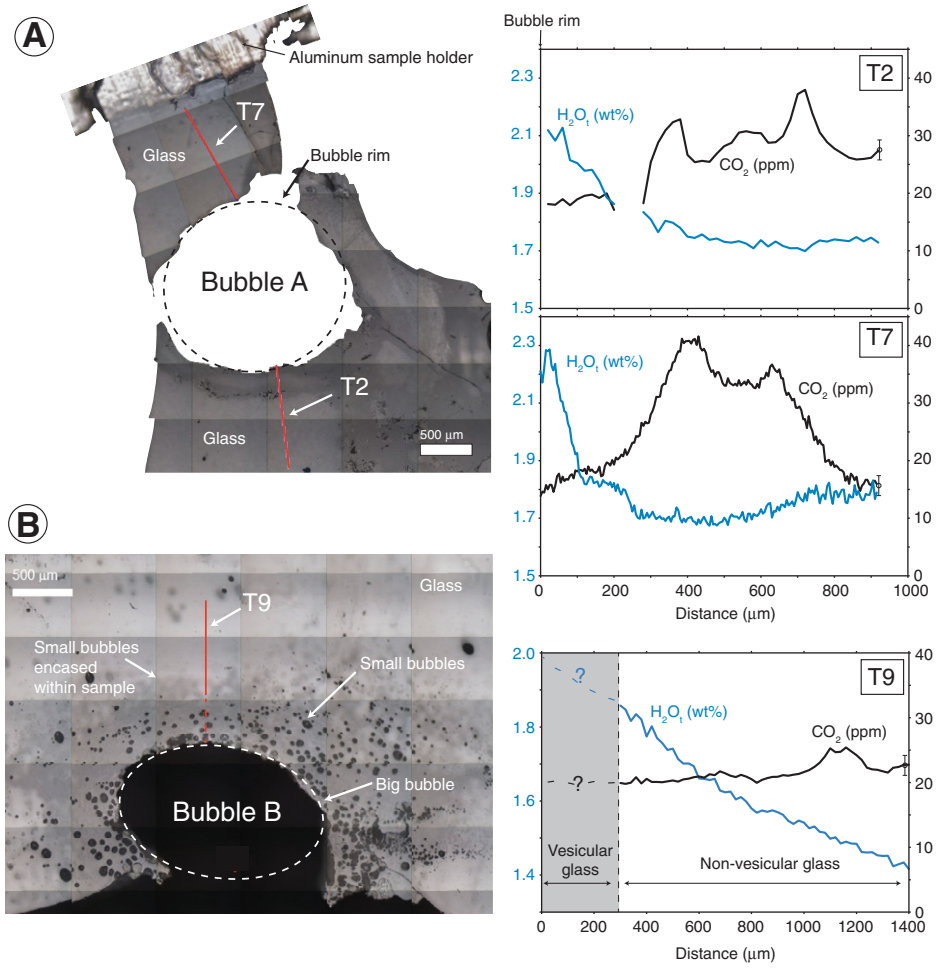

Figure 2. H_2O and CO_2 variations near bubbles. Photomosaics were taken using an infrared microscope camera at 10× magnification. A: Bubble A and locations of transects T2 and T7. Sample thickness is 177 µm. B: Bubble B and location of transect T9. There are no data in 300 µm surrounding bubble B, where H_2O and CO_2 have exsolved to form small bubbles. Sample thickness is 241 µm.

BUBBLE GROWTH AND RESORPTION

The observation that H_2O is enriched around some bubbles implies that these bubbles were resorbing into the melt. This is counter to the expectation that magma ascent should be accompanied by decompression-driven bubble growth. It is important that these enrichments were not overprinted to a significant extent during the final decompression associated with the eruption. We next assess the physical and chemical processes in the conduit that can explain the observed changes in H_2O solubility and bubble resorption.

Temperature Changes in the Conduit

Magma cooling at depth can cause bubbles to resorb because the solubility of water in rhyolite melt increases with decreasing temperature (T). At 30 MPa, a ΔT of ~300 °C would be required to increase water solubility from 1.7 to 2.2 wt% (Liu et al., 2005). The water enrichments could thus be attributed to isobaric cooling of magma in the conduit, but this interpretation does not explain the ring of bubbles around bubble B. Magma temperatures based on Fe-Ti oxide thermometry are between 790 and 910 °C (Carmichael, 1966); this places an upper bound of ~600 °C during bubble resorption. Since this is well below the glass transition temperature, where high viscosity prevents the formation of secondary bubbles, we conclude that cooling alone did not cause the observed water enrichments.

Pressure Changes in the Conduit

Obsidian welded to conduit margins can undergo multiple episodes of pressure changes due to cycles of brittle to viscous deformation (Tuffen et al., 2003; Gonnermann and Manga, 2003). The magnitude of pressure increase required to change the solubility of H_2O from 1.7 wt% to 2.2 wt% is ~10 MPa (Liu et al., 2005), comparable to the ΔP needed for fragmentation of melt with 10% porosity (Spieler et al., 2004; Romano et al., 1996). Brittle deformation of magma is favored at high strain rates, and the highest strain rates occur near conduit margins (Tuffen et al., 2003). After stress release, brecciated magma can reweld and deform viscously, allowing stress to reaccumulate. Thus, there is the potential for a clast of obsidian to have undergone repeated cycles of 5–30 MPa pressure changes (cf. Spieler et al., 2004, their figure 2).

The large variation in CO_2 concentration at the millimeter length scale requires a mechanism for frequently introducing new chemical heterogeneity. We interpret the variations in CO_2 as evidence of rewelded fracture surfaces or collapsed bubbles, near which CO_2 was depleted or within which CO_2 was enriched (cf. Rust et al., 2004; Castro et al., 2005; Cabrera et al., 2011). Since the diffusivity (D) of CO_2 is about an order of magnitude lower than that of H_2O in rhyolite liquid over the relevant temperature and pressure range (Zhang et al., 2007), we expect

[1]GSA Data Repository item 2012195, supplemental methods and a model for bubble dissolution, is available online at www.geosociety.org/pubs/ft2012.htm, or on request from editing@geosociety.org or Documents Secretary, GSA, P.O. Box 9140, Boulder, CO 80301, USA.

that heterogeneities in volatile concentration will persist longer for CO_2 than for H_2O. Therefore, while the H_2O data may be recording the final pressure increase prior to eruption, the CO_2 data may record previous cycles of fragmentation and annealing.

Chemical Changes in the Conduit

The solubility of water in rhyolite melt depends on melt and vapor composition. At a given pressure, an increase in the CO_2 content of the vapor leads to a decrease in H_2O solubility. Rust et al. (2004) attributed high CO_2/H_2O ratios in vesicle-free obsidian clasts to fluxing of a CO_2-rich fluid through the brecciated magma near conduit margins; they showed that equilibrium volatile loss, buffered by vapor of constant composition (X_{CO_2} = 0.07–0.25, where X_{CO_2} is the mole fraction of CO_2 in the vapor), can replicate the range of observed volatile contents in Mono Craters obsidian (blue curve in Fig. 1).

Vapor fluxing in this manner can lead to bubble resorption, but it does not explain the distribution of water around bubbles in Figure 2. Yoshimura and Nakamura (2010) conducted experiments that simulate a small parcel of magma surrounded by CO_2-rich fluid-filled fractures; in their experiments, water-rich bubbles resorb as CO_2 diffuses into the melt and water diffuses out. For bubbles resorbing by this mechanism, solubility changes are rate limited by CO_2 diffusion. Since $D_{H_2O}/D_{CO_2} \approx 10$, the expected signature is a depletion of CO_2 with uniform H_2O concentration around the resorbing bubble, which is not observed in Figure 2, but was observed experimentally (Yoshimura and Nakamura, 2010). Considering the distribution of CO_2 and the fact that water variations are uncorrelated with CO_2 variations, we attribute bubble resorption to pressure cycling in the conduit.

It is also important to consider the relatively low CO_2 contents in the 200 µm surrounding bubble A. There is no evidence that CO_2 is diffusing away from the bubble during the inferred recompression, suggesting that CO_2 is oversaturated and far from vapor-melt equilibrium. One possibility is that CO_2 is diffusing toward the bubble from the CO_2-rich regions further away, and that diffusion has not yet reached the bubble. An increase in the CO_2 content of the melt or vapor would serve to lower H_2O solubility, and in this scenario, the inferred pressure changes would represent a minimum estimate.

TIME SCALE FOR BUBBLE RESORPTION

Our data allow us to estimate pressure changes in the subsurface. Furthermore, H_2O concentration profiles can be used to quantify a time scale for pressure changes using a model for isothermal, diffusion-controlled bubble resorption. We do not attempt to model the CO_2 profiles because there is no clear choice of initial conditions and we do not know the CO_2 content of the bubble. Instead, we assume that the bubble is made entirely of water vapor and neglect effects of CO_2 concentration on water solubility. We assume that water diffusion begins after compression of the bubble and ceases upon quenching. This neglects bubble growth or water diffusion during the eruption and subsequent cooling, but these assumptions are supported by the absence of any significant decrease in H_2O near the bubble rim. Figure 3 shows the expected concentration profiles for a spherical bubble resorbing into an initially homogeneous melt (for a full description of the model, see the Data Repository). The concentration at 0 µm and 800 µm correspond to the equilibrium solubility of H_2O at P_f and P_i (final and initial), respectively (Liu et al., 2005). Once the initial conditions are set, the only input parameter is the diffusivity as a function of temperature, pressure, and composition. Initial and final conditions are provided in the figure. Since pressure is fixed at P_f during bubble resorption, the change in radius is due to mass loss alone.

Model results are compared to H_2O profiles from bubble A. Measured profiles are not symmetric about the bubble, and this may be due to one or more of the following: (1) the bubble is not spherical, (2) the melt shell surrounding the bubble may not have had uniform water content, or (3) one of the concentration profiles may have been affected by deformation. Nevertheless, the overall agreement between model and data suggests that diffusion-controlled bubble resorption can explain the main features of the measured H_2O concentration profiles. From the best fit we calculate a time scale of ~2–7 h for bubble resorption just prior to quenching. The time scale decreases by roughly a factor of 4 in going from 700 °C to 850 °C, and the range is in good agreement with the time scale for repeated fracturing and healing inferred from H_2O concentration profiles near healed fractures in pyroclastic obsidian (Cabrera et al., 2011), as well as the time scale between successive hybrid earthquakes at other silicic volcanic centers (Tuffen et al., 2003).

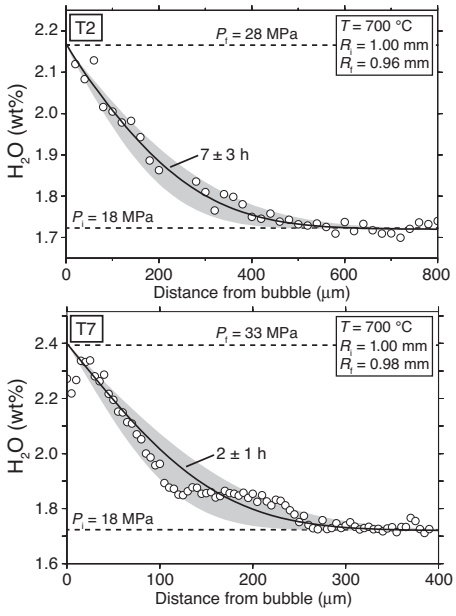

Figure 3. Model results for diffusion of water away from resorbing bubble. Comparison to data from T2 and T7 indicates that bubble A was resorbing for 2–7 h prior to eruption. *T*—temperature; *P*—pressure (i is initial, f is final), *R*—radius of bubble.

The inferred time scale of one to several hours is in accord with the observation that H_2O concentration profiles are relatively smooth whereas those for CO_2 are not. For bubble A, the length scale of CO_2 heterogeneities is ~100 µm, and these can be homogenized by diffusion in time, τ_d, ~30 h at T = 700 °C ($D_{CO_2} \approx 10^{-13}$ m²/s) ($\tau_d \sim L^2/D$, where L is the length scale over which concentration varies, and D is the diffusivity of CO_2.). Comparable heterogeneities in H_2O concentration can be homogenized by diffusion in <3 h ($D_{H_2O} \approx 10^{-12}$ m²/s).

IMPLICATIONS FOR DEGASSING

As shown in Figure 1, the path within the range of possible degassing paths, from open to closed system, and equilibrium to nonequilibrium, is difficult to resolve from existing data sets on sample suites. Samples with relatively high CO_2/H_2O ratios in Mono Craters obsidian clasts can be explained either by nonequilibrium degassing or equilibrium degassing in the presence of a CO_2-rich source at depth. In the nonequilibrium degassing model, slow diffusion of CO_2 into bubbles or fractures is used to explain elevated CO_2/H_2O ratios in the vesicle-free obsidian clasts.

There is little doubt that CO_2-rich vapors interact with shallow magma reservoirs at many volcanic centers (Yoshimura and Nakamura, 2011, and references therein), and our data do not rule out the presence of a CO_2-rich vapor in the Mono Craters system. However, can the chemical heterogeneities introduced by this mechanism reach an equilibrium distribution before melt is trapped in growing minerals or quenched to glass? To this end, the variability in volatile concentrations within individual pyroclasts is informative. The preservation of these volatile concentration gradients across clasts and near bubbles provides the first direct evidence for vapor-melt disequilibrium and suggests that nonequilibrium volatile loss at least contributes to, if not dominates, the signal of elevated and scattered CO_2/H_2O ratios in pyroclasts from Mono Craters.

Measurements of volatile concentration gradients may ultimately offer a means to distinguish between degassing models at Mono Craters and other volcanoes. The discovery of H_2O

concentration variations near welded fractures (Cabrera et al., 2011) suggests that direct evidence for CO_2-rich vapor fluxing might be preserved in concentration gradients near healed fractures. This will require relatively thick samples or samples with high enough CO_2 to make measurements. In addition, in places where volcanic gas emissions can be monitored, CO_2 fluxing might be detected by a monotonic decrease in emission rate accompanied by an increase in the CO_2 content of the vapor (Yoshimura and Nakamura, 2011).

BUBBLE GEOBAROMETRY

Volatile concentration gradients near bubbles in pyroclastic obsidian preserve a record of conduit processes. We interpret elevated H_2O concentrations near bubble rims as evidence of bubble resorption caused by an ~10 MPa pressure increase within the volcanic conduit just prior to eruption. This interpretation is appealing because it takes into account textural evidence for pressure changes due to repeated fragmentation and annealing of magma. We caution, however, that neither the shell of bubbles nor the enrichment in water may be common among bubbles in obsidian clasts. Furthermore, using bubbles to infer conduit dynamics requires that subsequent processes, such as volatile exsolution during decompression and eruption, do not overprint chemical records of bubble resorption.

A pressure change of 2 MPa (corresponding to a change in solubility of ~0.1 wt% H_2O; Liu et al., 2005) could be detected in H_2O concentration profiles around bubbles. Pressure fluctuations due to repeated fragmentation and annealing could also lead to cycles of bubble growth and resorption. The time scale of bubble resorption can be viewed as the time between successive fragmentation events, the last being the eruption. Using a bubble resorption model, we determined a time scale of hours at 700–850 °C. Since chemical diffusivities increase with magma temperature, it is less likely that similar water concentration profiles would be preserved in mafic lavas. Textures such as small bubbles around a larger bubble might provide the only record of pressure cycling in high-temperature melts.

ACKNOWLEDGMENTS

This work was supported by National Science Foundation grants EAR-1049662 and EAR-1050000. We benefited from discussions with A. Thomas, C. Huber, W. DeGruyter, and K. Cashman, and insightful reviews from P. Wallace and three anonymous reviewers. The Advanced Light Source is supported by the Director, Office of Science, Office of Basic Energy Sciences, of the U.S. Department of Energy under Contract No. DE-AC02-05CH11231.

REFERENCES CITED

Bachmann, O., Wallace, P., and Bourquin, J., 2009, The melt inclusion record from the rhyolitic Kos Plateau Tuff (Aegean Arc): Contributions to Mineralogy and Petrology, v. 159, p. 187–202, doi:10.1007/s00410-009-0423-4.

Blundy, J., Cashman, K., Rust, A., and Witham, F., 2010, A case for CO_2-rich arc magmas: Earth and Planetary Science Letters, v. 290, p. 289–301, doi:10.1016/j.epsl.2009.12.013.

Cabrera, A., Weinberg, R., Wright, H., Zlotnik, S., and Cas, R., 2011, Melt fracturing and healing: A mechanism for degassing and origin of silicic obsidian: Geology, v. 39, p. 67–70, doi:10.1130/G31355.1.

Carmichael, I., 1966, The iron-titanium oxides of salic volcanic rocks and their associated ferromagnesian silicates: Contributions to Mineralogy and Petrology, v. 14, p. 36–64, doi:10.1007/BF00370985.

Castro, J., Manga, M., and Martin, M., 2005, Vesiculation rates of obsidian domes inferred from H_2O concentration profiles: Geophysical Research Letters, v. 32, L21307, doi:10.1029/2005GL024029.

Gonnermann, H., and Manga, M., 2003, Explosive volcanism may not be an inevitable consequence of magma fragmentation: Nature, v. 426, p. 432–435, doi:10.1038/nature02138.

Gonnermann, H., and Manga, M., 2005, Nonequilibrium magma degassing: Results from modeling of the ca. 1340 A.D. eruption of Mono Craters, California: Earth and Planetary Science Letters, v. 238, p. 1–16, doi:10.1016/j.epsl.2005.07.021.

Johnson, E., Wallace, P., Cashman, K., Granados, H., and Kent, A., 2008, Magmatic volatile contents and degassing-induced crystallization at Volcán Jorullo, Mexico: Implications for melt evolution and the plumbing systems of monogenetic volcanoes: Earth and Planetary Science Letters, v. 269, p. 478–487, doi:10.1016/j.epsl.2008.03.004.

Liu, Y., Zhang, Y., and Behrens, H., 2005, Solubility of H_2O in rhyolitic melts at low pressures and a new empirical model for mixed H_2O-CO_2 solubility in rhyolitic melts: Journal of Volcanology and Geothermal Research, v. 143, p. 219–235, doi:10.1016/j.jvolgeores.2004.09.019.

Navon, O., Chekhmir, A., and Lyakhovsky, V., 1998, Bubble growth in highly viscous melts: Theory, experiment, and autoexplosivity of dome lavas: Earth and Planetary Science Letters, v. 160, p. 763–776, doi:10.1016/S0012-821X(98)00126-5.

Newman, S., and Lowenstern, J., 2002, VolatileCalc: A silicate melt-H_2O-CO_2 solution model written in Visual Basic for excel: Computers & Geosciences, v. 28, p. 597–604, doi:10.1016/S0098-3004(01)00081-4.

Newman, S., Epstein, S., and Stolper, E., 1988, Water, carbon dioxide, and hydrogen isotopes in glasses from the ca. 1340 A.D. eruption of the Mono Craters, California: Constraints on degassing phenomena and initial volatile content: Journal of Volcanology and Geothermal Research, v. 35, p. 75–96, doi.10.1016/0377-0273(88)90007-8.

Prousevitch, A., and Sahagian, D., 1998, Dynamics and energetics of bubble growth in magmas: Analytical formulation and numerical modeling: Journal of Geophysical Research, v. 103, p. 18223–18251, doi:10.1029/98JB00906.

Prousevitch, A., Sahagian, D., and Anderson, A., 1993, Dynamics of diffusive bubble growth in magmas: Isothermal case: Journal of Geophysical Research, v. 98, p. 22283–22307, doi:10.1029/93JB02027.

Roggensack, K., Hervig, R., McKnight, S., and Williams, S., 1997, Explosive basaltic volcanism from Cerro Negro Volcano: Influence of volatiles on eruptive style: Science, v. 277, p. 1639–1642, doi:10.1126/science.277.5332.1639.

Romano, C., Mungall, J., Sharp, T., and Dingwell, D., 1996, Tensile strengths of hydrous vesicular glasses: An experimental study: American Mineralogist, v. 81, p. 1148–1154.

Rust, A., Cashman, K., and Wallace, P., 2004, Magma degassing buffered by vapor flow through brecciated conduit margins: Geology, v. 32, p. 349–352, doi:10.1130/G20388.2.

Sieh, K., and Bursik, M., 1986, Most recent eruption of the Mono Craters, eastern central California: Journal of Geophysical Research, v. 91, p. 12539–12571, doi:10.1029/JB091iB12p12539.

Spieler, O., Kennedy, B., Kueppers, U., Dingwell, D., Scheu, B., and Taddeucci, J., 2004, The fragmentation threshold of pyroclastic rocks: Earth and Planetary Science Letters, v. 226, p. 139–148, doi:10.1016/j.epsl.2004.07.016.

Spilliaert, N., Allard, P., Metrich, N., and Sobolev, A., 2006, Melt inclusion record of the conditions of ascent, degassing, and extrusion of volatile-rich alkali basalt during the powerful 2002 flank eruption of Mount Etna (Italy): Journal of Geophysical Research, v. 111, B04203, doi:10.1029/2005JB003934.

Tuffen, H., Dingwell, D., and Pinkerton, H., 2003, Repeated fracture and healing of silicic magma generate flow banding and earthquakes?: Geology, v. 31, p. 1089–1092, doi:10.1130/G19777.1.

Yoshimura, S., and Nakamura, M., 2010, Chemically driven growth and resorption of bubbles in a multivolatile magmatic system: Chemical Geology, v. 276, p. 18–28, doi:10.1016/j.chemgeo.2010.05.010.

Yoshimura, S., and Nakamura, M., 2011, Carbon dioxide transport in crustal magmatic systems: Earth and Planetary Science Letters, v. 307, p. 470–478, doi:10.1016/j.epsl.2011.05.039.

Zhang, Y., Xu, Z., Zhu, M., and Wang, H., 2007, Silicate melt properties and volcanic eruptions: Reviews of Geophysics, v. 45, RG4004, 27 p., doi:10.1029/2006RG000216.

Manuscript received 16 November 2011
Revised manuscript received 15 February 2012
Manuscript accepted 25 February 2012

Printed in USA